Macromolecular Theory and Simulations

Macromolecular Theory and Simulations
www.mts-journal.de

RESEARCH ARTICLE OPEN ACCESS

Coupled Electro-Thermal and Mechanical Simulation of Radio-Frequency Welding of ETPU Bead Foams: A Multiphysics Approach and Its Experimental Validation

Marcel Dippold | Michael Scheiber | Holger Ruckdäschel

Department of Polymer Engineering, University of Bayreuth, Bayreuth, Germany

Correspondence: Holger Ruckdäschel (holger.ruckdaeschel@uni-bayreuth.de)

Received: 9 July 2025 | **Revised:** 12 August 2025 | **Accepted:** 14 August 2025

Funding: This research was funded by the "Bavarian Ministry of Economic Affairs, Regional Development and Energy" within the funding program "Verbundforschungsprogramm Förderlinie Materialien und Werkstoffe" (grant number MW-2104-0005).

Keywords: bead foams | electro-thermal simulation | ETPU | mechanical simulation | radio-frequency

ABSTRACT

Radio-frequency (RF) welding offers a promising, energy-efficient alternative to conventional steam-chest molding (SCM) for processing thermoplastic bead foams. This study presents a coupled electro-thermal and mechanical simulation model to predict the welding behavior and mechanical performance of expanded thermoplastic polyurethane (ETPU) bead foams. The model, implemented in COMSOL Multiphysics, incorporates temperature-dependent dielectric and mechanical properties. The electro-thermal simulation predicts spatial temperature distributions during RF welding and is validated by process-integrated temperature measurements and measured RF-generator power. These local temperatures are used to predict fusion quality at bead interfaces for subsequent mechanical simulation of tensile tests. The predicted stress distribution, crack formation, and failure behavior show good agreement with experimental results obtained via digital image correlation. The model reveals that surface cooling effects limit welding quality and mechanical strength despite sufficient core temperatures. The validated framework enables virtual process optimization and serves as a digital twin for predictive design of RF-welded foam parts. Future studies will extend the approach to other thermoplastic bead foams and integrate improved material models to enhance simulation accuracy.

1 | Introduction

Bead foams are a class of thermoplastic cellular materials composed of pre-expanded polymeric particles that are subsequently fused into complex three-dimensional structures [1]. Their unique processing method, which separates the foaming and molding steps, enables precise control over density, mechanical properties, and final part geometry for various applications. The production of bead foams typically follows two approaches: directly expanded beads, such as expanded polypropylene (EPP), where the foaming is simultaneous with the granulation, and expandable bead foams, such as expanded polystyrene (EPS), which are impregnated with blowing agents to allow controlled expansion at a later stage [2]. This flexibility reduces transport volume and enables on-demand density adjustment at the processing site. Bead foams offer low density, fine cell morphology, and excellent impact resistance, making them ideal for lightweight structural components, thermal insulation, and energy-absorbing applications. Classic examples include EPS in packaging and construction and EPP in automotive crash elements. More recently, expanded thermoplastic polyurethane (ETPU) has gained attention for its exceptional elastic recovery behavior, finding applications in high-performance sports equipment [2–4]. To fully exploit these

advantages, bead foams require efficient welding techniques to bond the individual particles into a three-dimensional structure [5]. While steam-chest molding currently is the dominant process for industry, alternative more energy-efficient methods are being explored to enhance process control and sustainability [6].

Among these processes, radio-frequency (RF) welding shows the greatest potential for large-scale processing of bead foams. Patented in 2017 by Kurtz GmbH, the process utilizes dielectric heating of the polymer through interaction with an oscillating electromagnetic field [7]. Unlike steam-chest molding, which relies on external heat transfer by the steam, RF welding enables volumetric heating of the polymer, reducing energy losses and providing direct process feedback. The RF welding setup consists of two electrodes connected to a high-frequency generator operating at 27.12 MHz [8]. The mold, typically made from insulating polymers like polytetrafluoroethylene (PTFE), prevents electrical short circuits while ensuring mechanical stability and defining the final part geometry [9]. Heating is governed by the material's dielectric properties, making the process inherently dependent on material composition and phase transitions [10]. However, challenges arise from inhomogeneous heating, particularly due to heat dissipation at the surface into the mold. To optimize welding quality, precise simulation-based electrode design and process control are necessary.

Complex physical problems with highly non-linear material properties, like within the RF process, cannot be solved analytically to receive the exact solutions, but require numerical methods in order to obtain high quality approximations [11, 12]. Amongst these approaches, the finite element method (FEM) is applicable to arbitrary problems in a wide field of natural and engineering science with no restrictions to geometry and nonlinear model equations [13]. The fundamental base of FEM is the discretization of the continuum volume into individual elements. These elements are defined by their nodes, possessing specific degrees of freedom for which the respective field variable is calculated through the solving process [14]. The accuracy of such numerical method is dependent on the element size, which is especially crucial in areas with high gradients of the field variable, e.g. around notches for structural simulations [13]. With rising computational powers over recent years, the complexity of these models can be increased in order to replicate the real process with high precision.

The simulation of the RF process and structural properties of the final bead foam samples is therefore a complex multiphysical approach with a stepwise coupled electro-thermal and mechanical problem to be solved.

The electromagnetic field solution is based on the Maxwell Equation (1), which are solved for the electromagnetic field strength $\vec{E}$ in a dynamic system [15, 16]. It is therefore determined by the wave number of the free space k_0, the relative permeability μ_r, and the relative permittivity ε_r^*. Losses due to the interaction of the electromagnetic field with the material are converted as volumetric sources of heat. The resulting temperature distribution across the model are therefore solved by the governing Equation (2) with the density of the material ρ, specific heat capacity C_p, and the thermal conductivity k [17].

$$\vec{\nabla} \times (\mu_r^{-1} \vec{\nabla} \times \vec{E}) - k_0^2 \varepsilon_r^* \vec{E} = 0 \tag{1}$$

$$\rho C_p \frac{\partial T}{\partial t} - \nabla \times (k \nabla T) - Q = 0 \tag{2}$$

Both parts of the simulation are solved in an iterative approach, so each model is based on the results of the others solved equations in a closed cycle until the convergence criteria are satisfied. Additionally, multiple material properties show a significant dependency on temperature throughout the process with direct influence on the resulting local bead fusion. Within this study, additional data from previous publications in combination with complementing measurements are used to create material models, which are used for simulation. The results of the electro-thermal and mechanical simulation are validated versus the real RF process and the mechanical testing of the samples under tensile load to analyze the welding quality between the individual beads. The paper provides new insights into the RF process and presents a holistic simulation model to improve the process and accelerate the adaptation of the technology to new material types. Thus, the study paves the way for increased sustainability in the production of lightweight parts made of bead foams.

2 | Experimental Section

2.1 | Material and Methods

As bead foam material, the commercially available ETPU grade Infinergy 32–100 U10 by BASF SE (Ludwigshafen, Germany) was used.

The beads show an average density of 183 kg/m^3 at an average equivalent diameter of 7.46 mm. The geometric analysis was done by a CAMSIZER ONLINE from the Microtrac Retsch GmbH (Haan, Germany).

For the electro-thermal simulation, the analysis of the dielectric properties versus temperature was performed with the RF I-V method with a E4991A RF impedance analyzer from Keysight Technologies, Inc. (Santa Rose, USA). More information about the detailed setup can be found in a previous study [10].

The heat capacity of the base polymer was analyzed by dynamic differential calorimetry (DSC) against a defined sapphire sample with known properties and an empty aluminum crucible. The measurement was performed from 20 up to 200°C with 20 K steps. The measurements were carried out with a Q 1000 by TA Instruments, Inc. (New Castle, USA).

Thermal conductivity of the foam material was measured at five temperatures between 20 and 85°C. This analysis was conducted by a HFM 446 Small from Erich NETZSCH B.V. & Co. Holding KG (Selb, Germany). A linear trend (R^2 = 0.9996) was used to extrapolate to higher temperatures.

In regard to the mechanical simulation, the properties of the foam volume inside the beads was assumed to be homogeneous

on a macroscopic scale. Reference samples of the same beads were welded via steam chest molding with optimized process parameters at a comparable density to ensure sufficient welding strength leading to predominant intra-bead failure. Thus, tensile tests of these samples provide the necessary input for tensile modulus, tensile strength, and Poisson's ratio of the bead volume. For the first two values, the reduction in cross-sectional area was taken into account to obtain true stress within the material. The adhesion of the bead was defined by a layered model. The temperature-dependent adhesion strength was used from a previous study up to a temperature of 140°C [18]. Complete healing of the interface is expected upon full melting of the crystalline regions followed by crystallization. At temperatures above 170°C, complete melting is assumed, which results in full healing of the interface. Consequently, the mechanical strength of the welded volume reaches the level of the polymer bulk material. The increase in strength between 140 and 170°C was directly correlated with the proportion of melted crystallites. For a quantitative analysis, the increase in strength was linearly correlated with the integral of the melting enthalpy over temperature.

2.2 | Radio-Frequency Welding

The welding of the bead foams was conducted by a Wave Foamer C from the manufacturer Kurtz GmbH & Co. KG (Kreuzwertheim, Germany). The setup can be investigated into detail in a previous study [19]. The power consumption of the generator, responsible for the applied oscillating voltage at the active electrode, was tracked. The temperature during welding and the subsequent cooling step was measured by a special fiberoptic sensor, due to interactions of the electromagnetic field with conductive materials. The sensor itself has an external diameter of 0.98 mm and is covered by an additional PTFE protective sleeve (outer diameter of 1.78 mm) for facilitated removal afterwards. The sensor was fixed with a small tape for positioning in the center of the plates. The actual position was always checked after the welding trials. Before manual filling of the mold, the beads had a temperature of 27°C and the mold was always preheated to 40°C in order to keep a constant starting temperatures. A stabilization time of 200 s was set to ensure sufficient cooling of the parts before demolding. The density of the final part was kept constant at 276 kg/m^3 (equals 25 vol.-% polymer) and controlled by weight before each welding trial. In order to prevent electrical arcing, the voltage increase was set over 2 s for all trials.

2.3 | Mechanical Characterization

The mechanical properties under tension are analyzed both for the steam-chest molding (SCM) reference plates as well as for the specimens produced via the RF process. For both variations, standardized test samples (DIN EN ISO 1798, geometry type 1A) were precisely cut out via a high-pressure water jet system. A minimum of 15 mm distance of the specimen to the edges of the welded plates was ensured in order to avoid edge effects. The test samples were conditioned at 23°C and 50 % relative humidity for at least 24 h prior to measurement. Testing of the samples was initiated with a 5 N pre-force and at a deformation-rate of 500 mm/min. Digital image correlation (DIC) was utilized to obtain local deformations within the area of constant cross-section, looking from the side on the previously cut flat surface (Figure 1).

A speckle pattern was applied beforehand manually by a spray can with black paint, increasing visibility for the DIC system. The frame rate of 10 Hz ensures a continuous analysis of the deformation up to the failure of the sample. During testing deformation was tracked via a digital strain gauge with a length of 40 mm placed within the linear middle section of the specimens and correlated with the stress obtained from the load cell and the cross sectional area. DIC was also utilized to measure Poisson's ratio over the elongation for the SCM reference plates.

3 | Model Development

Predicting the mechanical properties of a bead foam welded by RF technology takes a simulation model, which can combine different physics [20]. COMSOL Multiphysics (Version 6.3) by COMSOL Inc. (Burlington, USA) offers the opportunity to use and combine a wide range of physical models. Therefore, the software is widely used in academia and industry for complex multiphysical problems. The approach is split into two parts. In the first one, the heating during the welding process and subsequent cooling is simulated by coupling a thermal with an electrical module with the electromagnetic heating multiphysics. This proceeding ensures that for each step the electric field can be transferred into heat sources to calculate the initial local temperatures and material properties before the next step. The maximum temperature reached is subsequently used to set a local fusion strength for the bead interfaces, before the tensile test can be performed virtually in the second part of the simulation.

3.1 | Electro-Thermal Study

The initial electro-thermal simulation is performed separately with the entire geometry of the foam part, mold, electrodes and temperature sensor. As can be seen in Figure 2a, a symmetry plane through the sensor was used, dividing the geometry in half, to minimize computational time without compromising on result quality.

The geometrically simple model was built within COMSOL and dimensions were set according to the real geometries. The foam plate has a size of 200×200 mm^2 with a height of 10 mm. It is enclosed by a PTFE mold with a thickness of 20 mm to the upper and 10 mm to the lower electrodes and has a width of 40 mm around the foam part. Both electrodes are made of aluminum with a thickness of 5 mm, whereas the upper represents the active electrode where the oscillating voltage is applied and the lower one with ground potential applied. The voltage curve over time is obtained from the RF machine during testing and directly implemented into the simulation. The fiber optic sensor is modelled as a PTFE tube with a diameter of 1.78 mm and has a gallium arsenide core close to the tip to represent the real sensor as good as possible based on own optical analysis. As boundary conditions, an electrical and thermal isolation was set on the border of the geometry. The beads and mold had a starting temperature of 27 and 40°C, respectively.

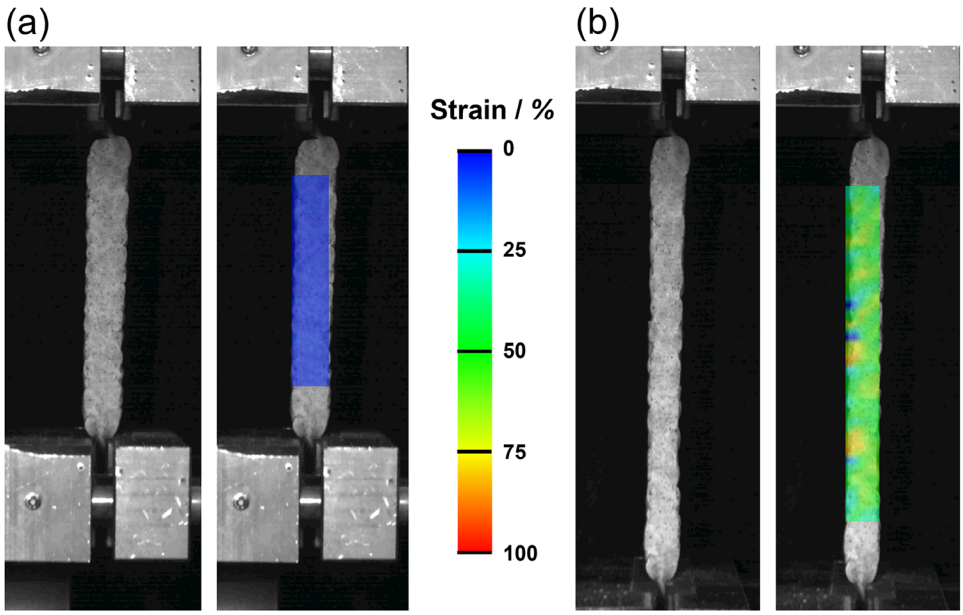

FIGURE 1 | Sideview on the tensile specimen during testing from the side by camera (a) and overlayed strain profile obtained by DIC (b).

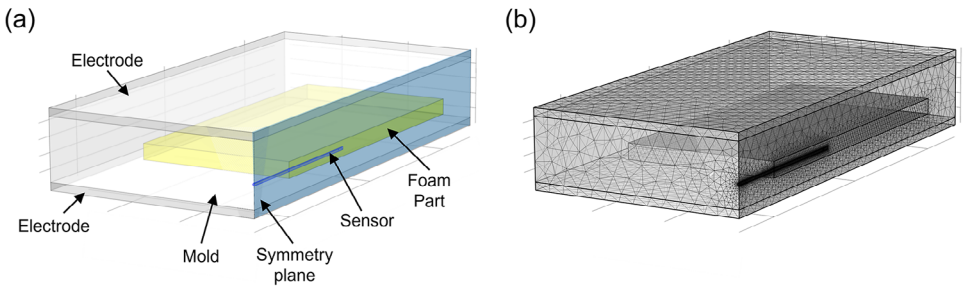

FIGURE 2 | Geometry model setup with electrodes (grey), mold (white), sensor (blue) and foam part (yellow) including the symmetry plane used (blue) (a) and meshed geometry (b).

Since adequate meshing is essential for high quality numerical results, a mesh refinement study was conducted initially. In order to limit computational time a locally adapted mesh was used as can be seen in Figure 2b. In areas with smaller feature sizes (sensor) and high importance (foam part) the mesh was specifically refined to obtain accurate results. In order to avoid local distortions from a non-uniform mesh, the element size within the foam part was set between 2 and 3 mm. Thus, resulting in a total number of 283 296 individual elements. The simulation was performed for a time frame of 100 s after the voltage was applied, so the initial cooling after welding can be observed as well.

Finally, the material model must be set up, including all relevant parameters partially with temperature dependency. As mentioned above, the main properties of the bead foams were analyzed in previous studies or in preparation. For the PTFE, aluminum and gallium arsenide, the properties were primarily adopted from build in material models within COMSOL and complemented with individual properties from data sheets.

As the simulation type a frequency-transient study was utilized to incorporate both the dependency on the oscillating voltage and heating over the process time. An implicit time-dependent solver type based on the BDF method was chosen with a maximum time step of 0.5 s. To overcome the multiphysical problem, a segregated solver approach was used splitting the electrical and thermal part into individual subproblems to be solved once at a time. The relative tolerance for the iterations was set at a value of 0.01.

3.2 | Mechanical Study

The mechanical properties of bead foams are highly dependent on the intricate interplay between the internal foam structure and the adhesion between the individual interfaces [21, 22]. Therefore, the foam part was statistically divided into individual segments based on the size distribution and shape obtained from analysis of the real material. The open source software Neper Version 6.10.1 was used for the tessellation of the volume as can be seen in Figure 3a.

For subsequent tensile testing, a type 1A specimen is cut out of the plate, representing the later geometry for the mechanical evaluation (Figure 3b). The resulting temperatures cannot be transferred from the previous study of the full mold assembly

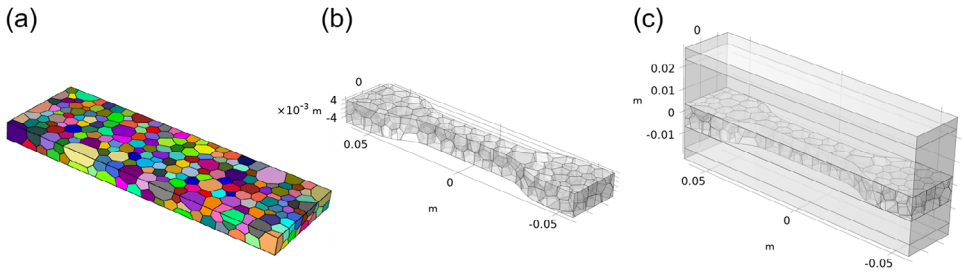

FIGURE 3 | Bead foam plate after tessellation into individual beads (a), the cut-out tensile specimen (b) and the entire model for the initial electro-thermal simulation (c).

due to the different geometries. Therefore, a separate electro-thermal study must be completed prior to the mechanical one. The selected setup is shown in Figure 3c and consists of the same arrangement of two electrodes, the mold and the bead foam part in the middle. To simplify the geometry, the cut out sections close to the middle part of the tensile bar were filled again to create a rectangular sample. All material models, boundary and starting conditions, and applied loads (voltage) are the same. Since only a small inner section of the whole assembly is considered to save computational resources by neglecting edge effects, thermal and electrical isolation is set as a boundary condition around the edges. The mesh size was reduced after an initial study to 1.3 – 2.0 mm, which is especially important for mechanical studies with crack development [23]. Besides the tessellation, the bead foam part in this first step is modelled as a continuous volume.

For the mechanical simulation, only the tensile specimen geometry is considered. The temperature-dependent adhesion between the beads is implemented by a thin layer model between the individual bead volumes. The strength of that layer is defined by the local temperature reached during the welding simulation and translated into strength by the temperature-dependent adhesion, as described before. The mechanical parameters (strain-dependent modulus and Poisson's ratio as well as ultimate tensile strength) for the bead volume are measured at the SCM plates, which showed predominant intra-bead failure. Both phases are simulated as linear elastic material and with an active damage model. The virtual tensile test was performed by fixing one side of the specimen and setting an increasing displacement on the other side up to 75 mm to ensure a failure. A stationary study type with an increasing deformation parameter was used to simulate the elongation of the sample.

4 | Results and Discussion

4.1 | Electro-Thermal Simulation and Experimental Validation

As described previously, the multiphysical electro-thermal simulation is divided into two separate subproblems being solved for each time step individually. For both parts, the respective field variable is calculated for each time step and can be visualized. In Figure 4, the irregular distribution of the electrical field strength can be seen between the electrodes.

This distortion is attributed to multiple overlaying effects based on geometrical aspects and differences in material properties [24, 25]. Therefore, the electrical field strength varies locally from the calculated $2.83 \times 10^5\ V/m$ for a homogeneously filled capacitor in both directions. First, the geometric setup of mold and foam can be roughly estimated by a simple equivalent circuit with capacitors in series and parallel. Thus, areas with lower permittivity cause an increased voltage-drop and therefore a higher field strength, which can be seen in the distribution after 5 s. In this stage of the process, the still cold foam part has a lower permittivity compared to the surrounding PTFE mold. Therefore, the voltage drop in the central area is significantly shifted to the foam part resulting in an increased field strength. A second effect can be seen at the edge of the part on the left and right side. Here, the difference in dielectric properties leads to a distortion of the field toward the mold and thus a reduced strength in the foam part close to the edge. With increasing process time, the dielectric heating leads to an increase in temperature of the foam part (Figure 5).

With higher temperatures, the permittivity of the foam part approaches that of the mold material. Thus, the electric field strength distribution appears more homogeneous across the assembly. Close to the surface, the inert mold leads to a significant cooling of the foam part. This can be seen both in the temperature distribution and has a direct effect on the field strength in this area. Despite showing constant volumetric heating in the foam, the contact to the mold therefore results in a colder surface compared to the center of the part, which represents one of the biggest challenges for the RF process. Another interesting area is the fiber-optic sensor in Figure 5. Due to its inert nature and higher thermal mass compared to the surrounding foam, it stays significantly colder during the welding process and lags behind. This fact must be considered in the evaluation of the measured temperature data.

In order to test the accuracy of the simulation model, power curves over time can be compared, representing a direct process-feedback based on the changing permittivity of the foam material throughout the welding process. In Figure 6, the data from the real measurements, as obtained from the RF device, is compared to the simulation data at 6 and 8 kV with varying welding times at maximum voltage.

As expected, the simulated curves are perfectly overlapping until the voltage is cut off at the end of each trials. The overall trend shows good agreement to the real measurements with an initial peak in power slightly after the voltage curves reaches their desired maximum value after around 4 s followed by a steep decline toward the end. This is perfectly in line with the

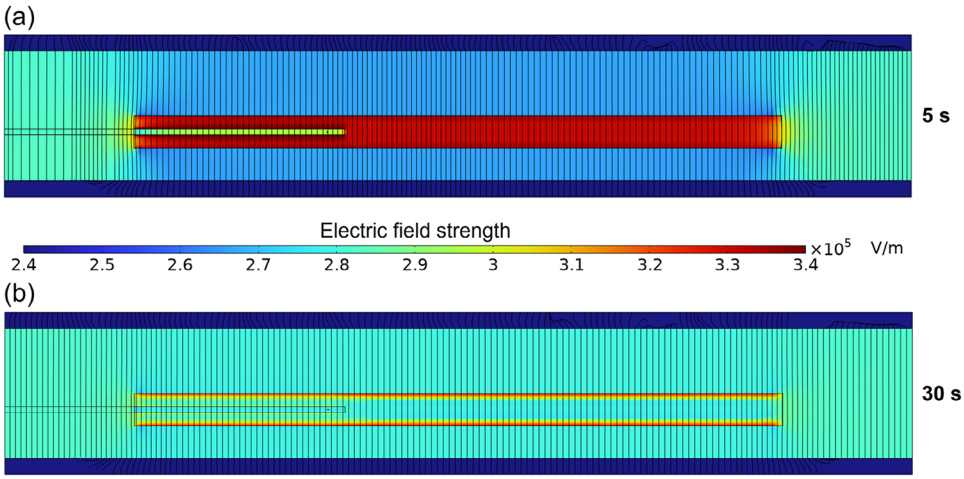

FIGURE 4 | Cross section of the simulation model with electric field strength after 5 s (a) and 30 s (b) for the simulated trial at the welding parameters of 8 kV for 35 s.

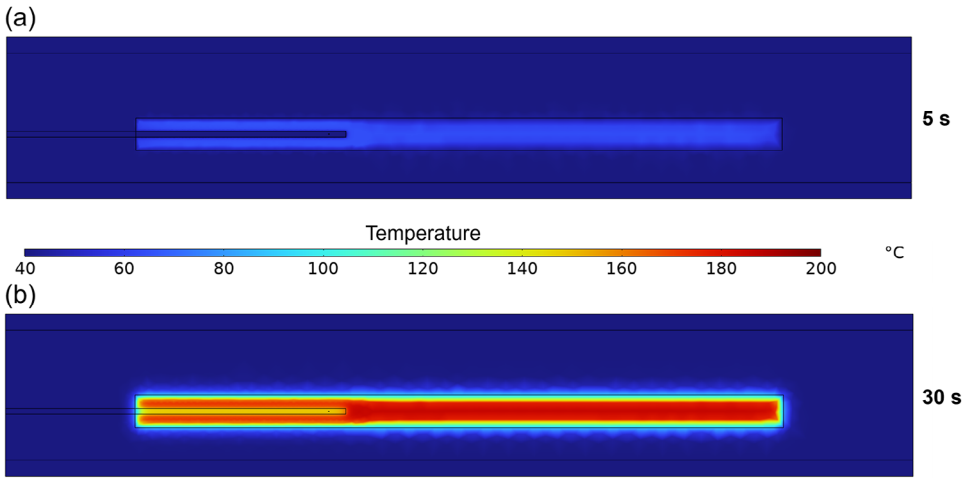

FIGURE 5 | Cross section of the simulation model with temperature distribution after 5 s (a) and 30 s (b) for the simulated trial at the welding parameters of 8 kV for 35 s.

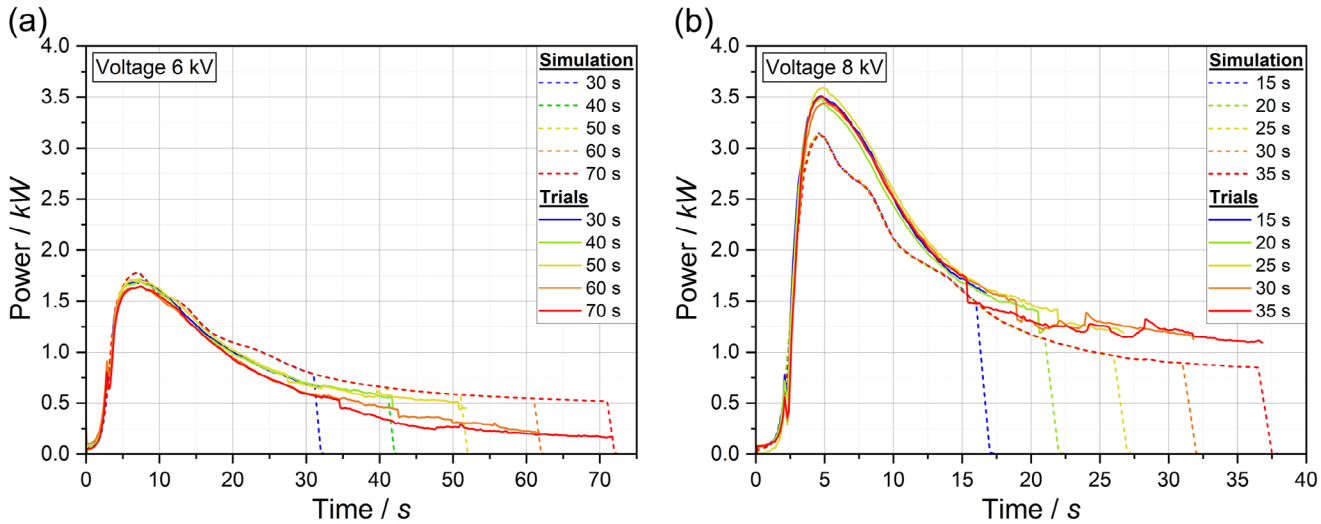

FIGURE 6 | Power curves over fusion time from real trials and simulation at a voltage of 6 kV (a) and 8 kV (b).

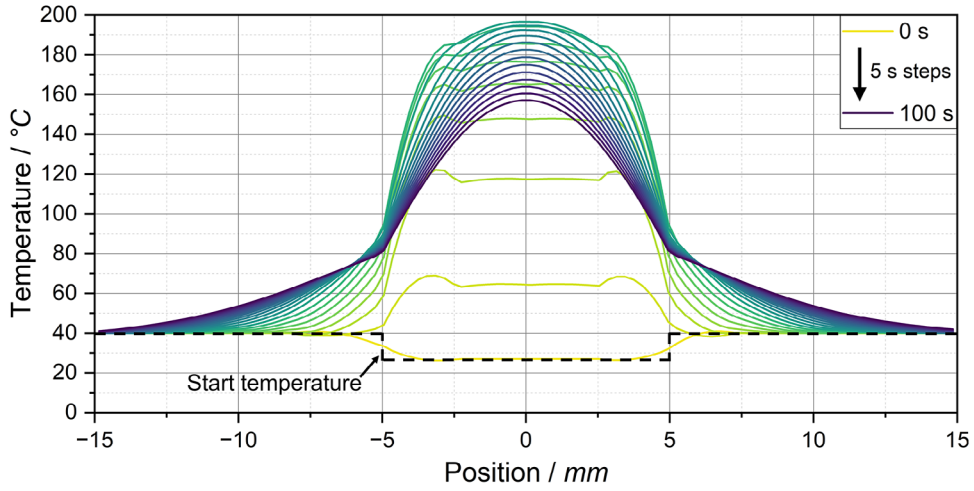

FIGURE 7 | Temperature distribution across the height (0 mm equals center of the 10 mm foam plate) from 0 to 100 s in 5 s steps for the simulated trial at 8 kV 35 s.

temperature-dependency of the imaginary part of the complex permittivity, as discussed previously. During the real measurements, jumps within the power curves are visible toward the later stages, which may not be attributed to actual changes in the material. This is probably caused by fluctuations in internal data recording or changes in the generator or the control system. Deviations to the simulated curves to later times can therefore be partially explained. Overall the simulation agrees well with real measurements, especially in the earlier stages close to the maximum power input. Since the power curves depend on the average properties of the entire setup, local effects cannot be resolved.

For the final goal of a homogeneous welding quality across the foam beads within the entire part, the temperature distribution is the key factor. In comparison to a punctual measurement of the temperature in the real trials, the virtual representation allows a consistent analysis throughout the volume. In order to visualize both the distribution of temperature across the plate thickness and inside the mold as well as the changes during the welding time, a temperature profile at individual time steps is presented in Figure 7.

In the beginning at 0 s, the initial starting temperatures of 40°C in the mold and 27°C for the foam beads can be observed. At the interface, the meshing leads to individual nodes being influenced by both starting temperatures. Therefore no distinct step is evident, thus resulting in a transition between the two areas. Over time, the volumetric heat input into the foam results in an increase in the temperature profile, reaching its maximum at 35 s. Again, the inhomogeneity between the hot core and the colder surface can be seen. Due to its higher thermal mass, the mold only heats up slightly to a maximum of 90°C on the surface. For a continuous production process the change in mold temperature must be investigated further since deviations between the cycles will lead to differences in part quality. For a safe demolding of the part without damage, a limited temperature must be reached to ensure a sufficient mechanical stability of the foam part. These two factors will significantly determine the cycle time of the RF process and can be predicted or optimized by the digital twin.

For improved comparability with the real measurements, the time-dependent temperature curves at different positions as well as the simulated and real sensor can be observed in Figure 8.

First, the power input from Figure 6 can be translated into heating rates, which can be seen at the curves close to the center of the foam plate at 0 mm distance. Closer to the surface of the part, the cold mold significantly influences the heating, thus resulting in lower temperatures. Second, the data obtained from the real fiber-optic sensor shows a significant lag behind the simulated temperature by reaching its maximum approx. 10 s later for this parameter set. By modelling the sensor in numerical simulation, the behavior can be produced precisely showing the same trend over time. In combination with the power curves, these results indicates the conformity of the presented simulation model. Besides the overall curve, the maximum temperature reached represents the key parameter for a high quality bead welding without damage of the cellular structure. By comparing the maximum temperatures reached for the simulated and real sensor at varying welding parameters in Figure 9, a good agreement is observed.

Additionally, the significant difference between the temperature measured by the sensor with the simulated actual foam temperature can reach up to 20 K. This underlines the importance of a validated simulation not only for predictive reasons, but also in order to get a deeper knowledge of the material process interactions, especially for the highly temperature-dependent welding phase.

4.2 | Mechanical Simulation and Experimental Validation

The electro-thermal simulation provides the basis for the subsequent mechanical simulation. Both parts are connected via the temperature-dependent welding strength, which is locally set for the bead interfaces. The virtual samples were tested under tensile deformation until failure. As can be seen in Figure 10 on the left side, without external deformation the sample shows no stress.

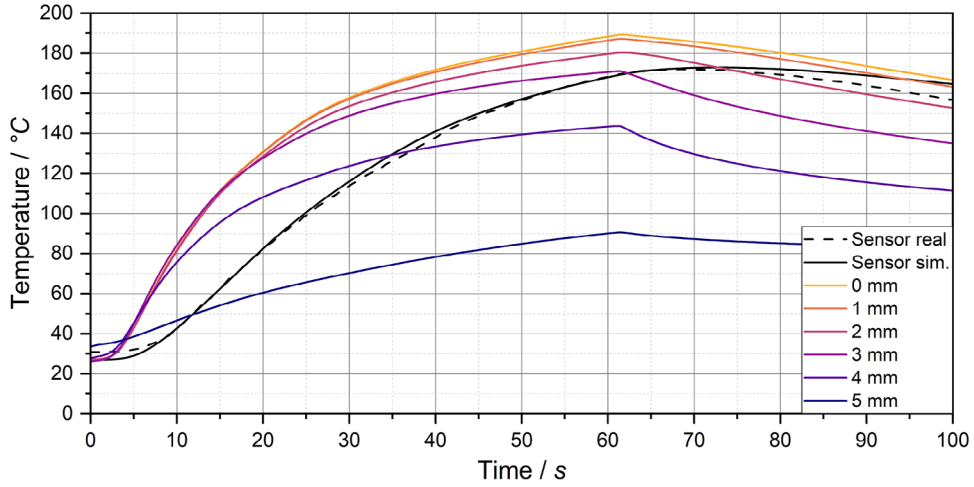

FIGURE 8 | Temperature development over time for the real and simulated sensor as well as for the simulation at different positions in relation to the center directly in the foam at 6 kV 30 s.

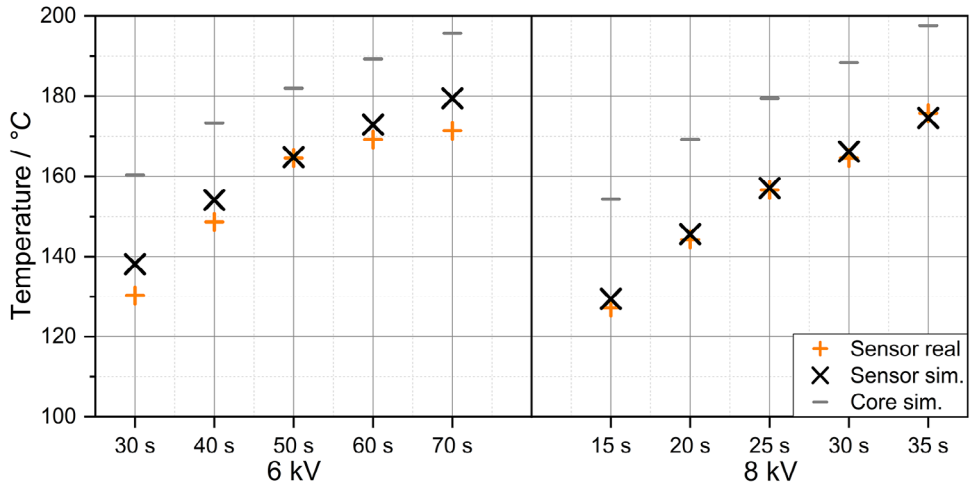

FIGURE 9 | Comparison of the temperature peak for all trials obtained from the real sensor and from the simulation at the virtual sensor and directly in the center of the foam.

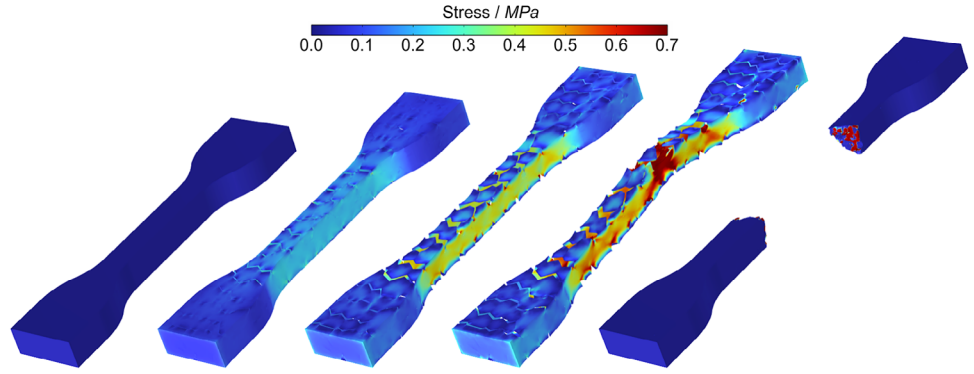

FIGURE 10 | Graphical representation of the virtual tensile test at different stages of deformation until failure of a sample welded at 6 kV for 30 s.

Due to the increased elongation of the sample, mechanical stress is induced. At minor deformations, the first surface cracks are visible originating from insufficient welding between the beads in these areas. These cracks hinder the transfer of forces in the outer areas, resulting in reduced stress. This influences the cross-section effective for load transfer of the welded samples and therefore impacts the measured mechanical properties. At a certain point of deformation, the stress, especially in the notches due to the surface cracks, is too high. As a result, the rest of the sample fails through the bead volume. After failure, no

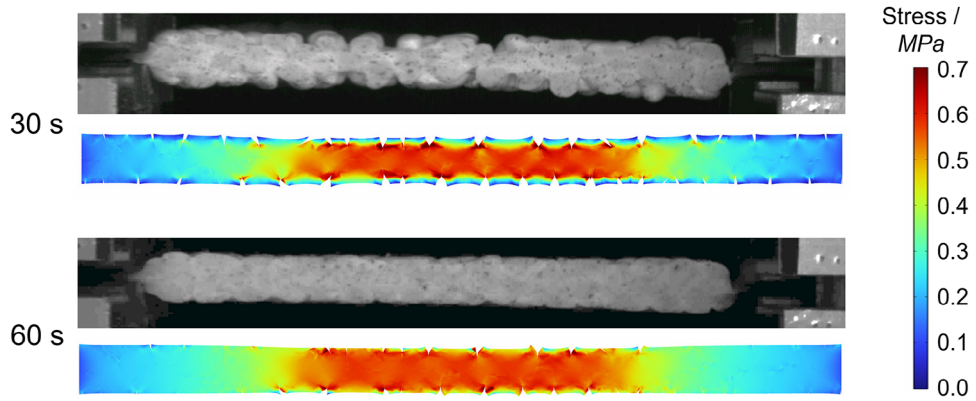

FIGURE 11 | Comparison of the lateral view of tensile samples welded at 6 kV for 30 and 60 s in reality and simulation at a similar deformation.

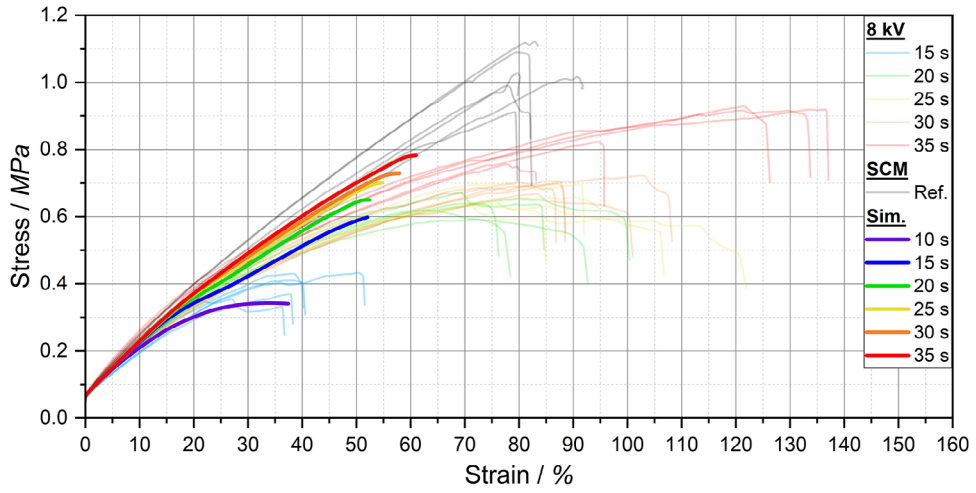

FIGURE 12 | Comparison of the stress-strain curve of the real and simulated tensile tests for samples welded at 8 kV including the SCM reference.

physical connection between the two parts is present, thus stress is relieved.

The results from the mechanical simulation can be validated on an optical comparison with the real tests. In Figure 11, the side view on the tensile sample at similar deformation is shown.

Based on the inhomogeneity in temperature due to the cold mold, the beads in proximity to the surface don't reach a sufficient temperature for welding. This results in pronounced crack formation for the sample at 30 s of welding time. Increasing the welding time to 60 s, higher temperatures are reached toward the surface of the foam part, leading to enhanced welding quality and reduced cracks. The build-up simulation can nicely represent the real observations for both processing parameters. At 30 s the outer foam beads show a significant spring back effect during the opening of the mold. This geometric changes of the tensile samples, which will influence the resulting mechanical properties, cannot the predicted with the current simulation model.

Additionally, the classical stress-strain curve can be compared with the real tests and their virtual representation (Figure 12).

The results show a significant influence of the previous welding parameters on the behavior of the samples, with increasing strength and maximum strain for longer welding times. At low strains, the curves match the real measurements nicely. Especially for higher welding times and therefore increased maximum temperatures, the real strain-curves flatten. This can be explained by a change in the material properties due to partial melting of the core areas, which has been confirmed by thermal analysis of the melting behavior from the inside of the welded plates. Because of this change in material properties due to changes in crystalline structure and cellular morphology, the stiffness of the material is highly reduced leading to significantly higher strain at break. An adjusted material model would be necessary in order to take these process-dependent material changes into account. Compared to the SCM reference, which was used as input for the mechanical properties of the foam volume inside the beads, the simulated curve for the RF samples show lower stress at failure. This phenomena can be attributed to the crack initiation in the surface and therefor reduced effective cross-sectional area. The comparison of the resulting tensile strength from the real and simulated samples including the SCM reference also underpins the good conformity of the simulation (Figure 13).

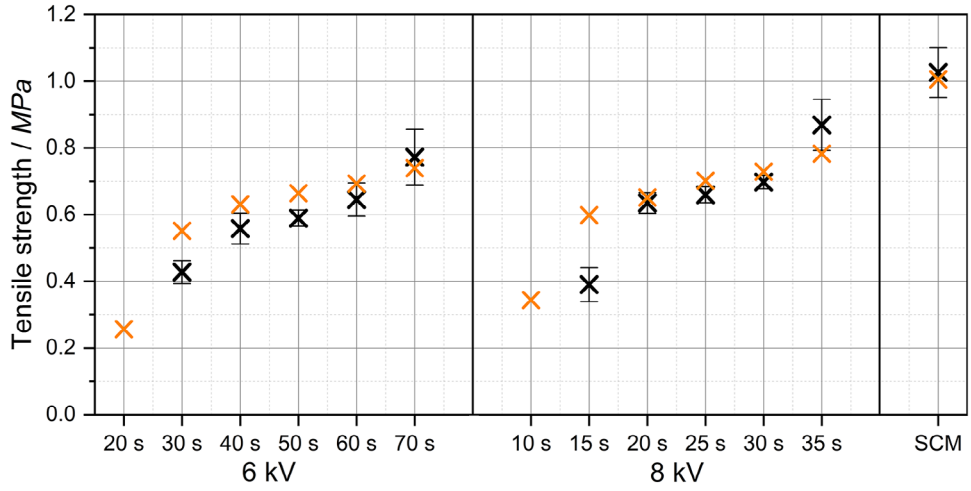

FIGURE 13 | Tensile strength of the simulated and real samples for varying RF parameters and SCM reference.

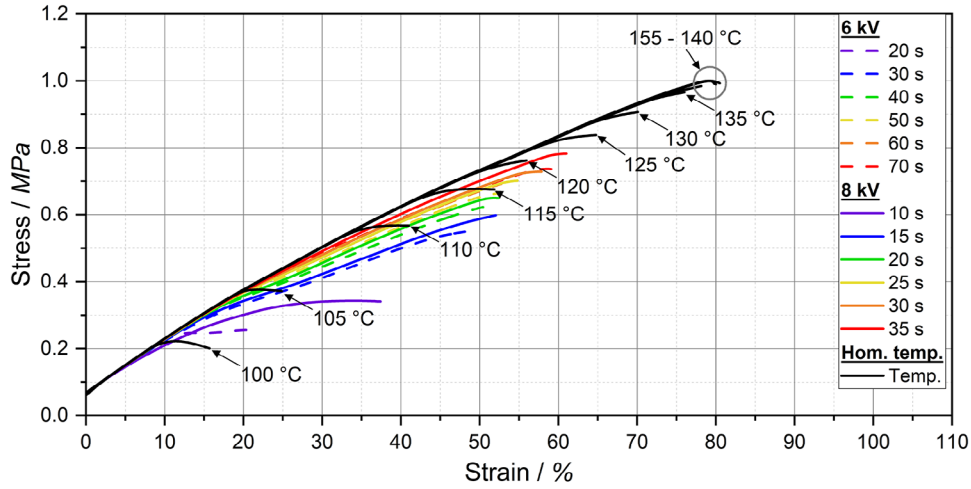

FIGURE 14 | Comparison of the stress-strain curves of the virtual tensile tests from the RF process and at a homogeneous temperature for welding.

Only at the lowest welding times per voltage, which resulted in stable plate in reality, the digital twin overestimated the tensile strength. This effect can be explained by the previously described geometric changes due to the spring-back effect close to the surface, resulting in more significant cracks and a homogeneous surface structure. For both voltages at the intermediate welding times, the predicted tensile strength by the simulation is within an error of less than 13 %. A further reduction in welding time to 20 s and 10 s, respectively, shows a significant drop in mechanical properties underlying the good representation of the behavior by the simulation.

To further test the capabilities of the numerical model, the mechanical simulation was tested in predicting performance of samples welded at homogeneous temperatures representing conditions close to SCM. In Figure 14 the simulated stress curves at different homogeneous temperatures are compared to experimental values of RF welded samples.

Due to the homogenous welding quality across the thickness, no premature crack initiation occurs. Therefore, the curve remains consistent until the overall stress within the sample causes complete failure of the specimen. At temperatures of 140°C and above the welding strength between the beads is sufficient enough to not limit the overall mechanical performance of the sample. At these welding temperatures the weakest link is the maximum strength of the foam volume inside the beads. The significant influence of the crack initiation in the surface compared to the overall welding in the inside of the plates can be observed by comparing these results to the maximum temperatures reached in the core in Figure 9. At 120°C of homogeneous welding, similar tensile strength can be obtained than with the highest welding times with RF, which showed significantly higher temperatures in the core. The surface is therefore crucial for the mechanical properties of samples produced via RF technology. Overall these results show the good agreement between the simulation model and real tests.

5 | Conclusions

In this study, a coupled electro-thermal and mechanical simulation approach was developed and validated to predict the welding quality and mechanical performance of expanded

thermoplastic polyurethane (ETPU) bead foams processed by radio-frequency (RF) welding. The multiphysics model incorporates temperature-dependent material properties and enables a spatially resolved prediction of the temperature field and resulting inter-bead adhesion within the foam structure. The electro-thermal model accurately reflects the spatial evolution of temperature during the RF process and demonstrates strong agreement with experimentally measured power and temperature data. The observed deviations of the measured sensor values were successfully explained by the thermal inertia of the optical fiber sensor, which was also replicated in the simulation with less than 8 K deviation. The mechanical simulation, based on a tessellated representation of the bead structure and locally defined interface strength, effectively captures the stress distribution, crack initiation, and ultimate failure of RF-welded tensile specimens. The model shows good agreement with experimental tensile test results across different welding parameters and accurately predicts the influence of inhomogeneous temperature distributions on mechanical performance. Especially for intermediate welding times, which resulted in the highest quality plates, the numerically predicted tensile strength was within a deviation of 13 %. Furthermore, the simulation reveals that welding quality, especially near the surface region, is critical for the mechanical integrity of the final part and cannot be deduced solely from core temperature data. The developed digital twin thus provides a powerful tool for understanding and optimizing the RF welding process of bead foams. It enables predictive adjustments of process parameters and supports the design of energy-efficient and high-performance lightweight components. This work lays the foundation for future studies on process scaling, cycle time optimization, and integration into closed-loop control systems for sustainable industrial application of RF welding technology. For the future extension of the approach, a transfer to other materials with higher welding temperatures or lower polarity, where further additives must be used, will need to be conducted. Additionally, the mechanical study shows significant changes of the bead volume properties due to overheating, which should be investigated more deeply and implemented into the material model.

Acknowledgements

The authors would like to acknowledge the Bavarian Polymer Institute (BPI) for providing access to the scanning electron microscope for optical analysis of the beads, which was not included in the paper due to limited space. This research was funded by the "Bavarian Ministry of Economic Affairs, Regional Development and Energy" within the funding program "Verbundforschungsprogramm Förderlinie Materialien und Werkstoffe" (grant number MW-2104-0005).

Open Access funding enabled and organized by Projekt DEAL.

Conflicts of Interest

The authors declare no conflicts of interest.

Data Availability Statement

The data that support the findings of this study are available from the corresponding author upon reasonable request.

References

1. D. Raps, N. Hossieny, C. B. Park, and V. Altstädt, "Past and Present Developments in Polymer Bead Foams and Bead Foaming Technology," *Polymer* 56 (2015): 5–19.

2. J. Jiang, B. Chen, M. Zhou, et al., "A Convenient and Efficient Path to Bead Foam Parts: Restricted Cell Growth and Simultaneous Inter-bead Welding," *The Journal of Supercritical Fluids* 194 (2023): 105852.

3. J. Meuchelböck, C. Peiffer, L. Walter, M. Dippold, P. Munro, and H. Ruckdäschel, "Influence of Temperature on the Compression Properties of Expanded Thermoplastic Polyurethane (ETPU)," *Journal of Materials Science: Materials in Engineering* 19 (2024): 10.

4. C. Ge, Q. Ren, S. Wang, W. Zheng, W. Zhai, and C. B. Park, "Steam-Chest Molding of Expanded Thermoplastic Polyurethane Bead Foams and Their Mechanical Properties," *Chemical Engineering Science* 174 (2017): 337–346.

5. J. Gensel, C. Pawelski, and V. Altstädt, "Welding Quality in Polymer Bead Foams: An in Situ SEM Study," *AIP Conference Proceedings* 1914 (2017): 060001.

6. J. Kuhnigk, T. Standau, D. Dörr, C. Brütting, V. Altstädt, and H. Ruckdäschel, "Progress in the Development of Bead Foams – A Review," *Journal of Cellular Plastics* 58 (2022): 707–735.

7. V. Romanov, Device and Method for Producing a Particle Foam Part, WO 2017/125412 A1 (2017).

8. K. Schneider, T. Kleffel, and D. Drummer, "RF Welding of Dielectric Lossless Foam Particles by the Application of a Dielectric Heatable Coating With High Recycling Potential," *Polymers* 15 (2023): 3950.

9. K. Schneider, B. Gothe, M. Drexler, et al., "The Effect of Dielectric and Thermal Properties of Plastic Mold Materials on the High Frequency Welding of Three-Dimensional Foam Components," *Polymer Engineering & Science* 62 (2022): 3400–3411.

10. M. Dippold, C. Töpfer, and H. Ruckdäschel, "Influence of Dielectric Properties of Polybutylene Terephthalate and Respective Foam Beads on Process Behavior in Radio-Frequency Welding," *Journal of Applied Polymer Science* 141 (2024): 1–12.

11. Y. Lyu, *Finite Element Method* (Springer Nature Singapore, 2022).

12. D. T. Nguyen, *Finite Element Methods* (Springer Nature Switzerland, 2024).

13. D. Dinkler and U. Kowalsky, *Introduction to Finite Element Methods* (Springer Vieweg Wiesbaden, 2024).

14. S. Unnikrishnan Nair and S. Somanath, *Introduction to Finite Element Analysis* (Springer Nature Singapore, 2024).

15. S. Grabmaier, M. Jüttner, D. Vögeli, W. M. Rucker, and P. Göhner, "Numerical Framework for the Simulation of Dielectric Heating Using Finite and Boundary Element Method," *International Journal of Numerical Modelling: Electronic Networks, Devices and Fields* 31 (2018): 1–8.

16. R.-J. Chen, N. Qiao, M. Arowo, et al., "Modeling for Temperature Distribution of Water in a Multiwaveguide Microwave Reactor," *Industrial & Engineering Chemistry Research* 59 (2020): 4762–4774.

17. Y. Alpert and E. Jerby, "Coupled Thermal-Electromagnetic Model for Microwave Heating of Temperature-Dependent Dielectric Media," *IEEE Transactions on Plasma Science* 27 (1999): 555–562.

18. M. Dippold, A. Himsel, J. Kuhnigk, M. Chairopoulou, M. Drexler, and H. Ruckdäschel, "Bead-to-Bead Analysis: Introducing an Innovative Methodology for Accelerated Quantitative Analysis of the Welding Behavior of Bead Foams," *Journal of Polymer Science* (2024): 1–8, https://doi.org/10.1002/pol.20240830.

19. M. Dippold, M. A. Chairopoulou, M. Drexler, M. Scheiber, and H. Ruckdäschel, *From Vibrating Molecules to a Running Shoe: Connecting Dielectric Properties With Process Feedback in Radio-frequency Welding of TPU Bead Foams* (2024), https://doi.org/10.51573/Andes.PPS39.GS.PFM.1.

20. K. Schneider, C. Ott, and D. Drummer, "Simulative Study of Polymeric Core–Shell Foam Particles for the Enlargement of the Material Portfolio in

3-D High-Frequency Welding," *Polymer Engineering & Science* 62 (2022): 486–496.

21. J. Jiang, F. Liu, X. Yang, et al., "Evolution of Ordered Structure of TPU in High-Elastic State and their Influences on the Autoclave Foaming of TPU and Inter-Bead Bonding of Expanded TPU Beads," *Polymer* 228 (2021): 123872.

22. P. Gahlen and M. Stommel, "Modeling of the Local Anisotropic Mechanical Foam Properties in Polyisocyanurate Metal Panels Using Mesoscale FEM Simulations," *International Journal of Solids and Structures* 244-245 (2022): 111595.

23. J. Baumgartner and T. Bruder, "An Efficient Meshing Approach for the Calculation of Notch Stresses," *Welding in the World* 57 (2013): 137–145.

24. F. Kremer and A. Schönhals, *Broadband Dielectric Spectroscopy* (Springer Berlin Heidelberg, 2003).

25. A. Küchler, *High Voltage Engineering* (Springer Vieweg Berlin, Heidelberg, 2018).